

This is a repository copy of *Solar cells micro crack detection technique using state-of-the-art electroluminescence imaging*.

White Rose Research Online URL for this paper:  
<https://eprints.whiterose.ac.uk/177700/>

Version: Accepted Version

---

**Article:**

Dhimish, Mahmoud and Holmes, Violeta (2019) Solar cells micro crack detection technique using state-of-the-art electroluminescence imaging. *Journal of Science: Advanced Materials and Devices*. pp. 499-508. ISSN 2468-2284

<https://doi.org/10.1016/j.jsamd.2019.10.004>

---

**Reuse**

This article is distributed under the terms of the Creative Commons Attribution-NonCommercial-NoDerivs (CC BY-NC-ND) licence. This licence only allows you to download this work and share it with others as long as you credit the authors, but you can't change the article in any way or use it commercially. More information and the full terms of the licence here: <https://creativecommons.org/licenses/>

**Takedown**

If you consider content in White Rose Research Online to be in breach of UK law, please notify us by emailing [eprints@whiterose.ac.uk](mailto:eprints@whiterose.ac.uk) including the URL of the record and the reason for the withdrawal request.

# Solar cells micro crack detection technique using state-of-the-art electroluminescence imaging

**Abstract:** in this article, we present the development of novel technique that is used to enhance the detection of micro cracks in solar cells. Initially, the output image of a conventional electroluminescence (EL) system is determined and reprocessed using a binary and discrete Fourier transform (DFT) image processing models. The binary image is used to enhance the detection of the cracks size, position and orientation, principally using the geometric properties of the EL image. On the other hand, the DFT has been used to analyse the EL image in two-dimensional spectrum. The output image of the DFT consists of structures of all required frequencies, hence, improve the detection of possible cracks presents in the solar cell. As a result, the developed technique improves the detection of micro cracks in solar cells compared to conventional EL output images.

**Keywords:** Solar Cells; EL Imaging; Micro cracks; Photovoltaics.

## 1. Introduction

Today, silicon photovoltaics (PV) modules are a very mature and advanced technology. Crystalline silicon (c-Si) PV modules share over 90% of the global PV market [1] reaching over 110 GW in 2018. Worldwide, with increasing number of PV installations, some of which are already more than 15 years in operation [2], multiple key challenges and new research fields have emerged. For a very successful and stable PV installation process, the knowledge about its performance under real environmental conditions is of high importance. In addition, PV grid operators' necessity to understand the current and the future PV electricity production, hence, to provide a reliable power supply to existing consumers. Therefore, it is very important to advance the present acquaintance of degradation mechanisms in PV modules.

One of the degradation mechanism is PV solar cells micro cracks [3]. Micro cracks are caused due to various reasons, including, but not limited to, the fluctuations in the surface temperature of solar cells [4], humidity variations between the rear and front side of the PV modules [5], present of partial shading including dust, clouds and permanent opaque objects [6]. While, the present of micro cracks in solar cells would cause a decrease in the overall output power generation of the affected PV modules, resulting a considerable decrease in the efficiency of the PV installations.

Different research show that the loss in the output power is permanently greater than 2.5% due to the present of micro cracks [7]-[9]. On the other hand, the case study done by M. Dhimish *et al.* [10] approves that the maximum power loss is equal to 20% for PV modules affected by multiple micro cracked solar cells. On the other hand, it is worth noting that PV micro cracks increase the degradation rate of PV modules in the range of -0.2%/year, based on the observations of A. Dolara *et al.* [11] and M. Florides *et al.* [12]. Therefore, the analysis and detection techniques of micro cracks are of high importance due to their impact on the PV modules reliability, durability, and output power performance alike.

The standard practice in current research & development (R&D) as well as manufacturing processing units (MPUs) to detect possible cracks in solar cells is using

the electroluminescent (EL) imaging technique [13]-[15]. EL imaging measures the radiative recombination of the solar cell under forward bias conditions, while this technique is comparatively less expensive than UV-Fluorescence detection method [16]. A brief overview of a typical EL imaging setup will be discussed later in sections 2 and 3.

There are several attempts to enhance the visibility in the observations and detection of micro cracks using the EL method. D. Tsai *et al.* [17] developed an automatic defect detection scheme based on Haar-Like feature extraction of a typical EL image. The technique has shown a fairly good detection rate of micro cracks, while the computational time is limited to 0.1s for a 550 x 550 image resolution. A faster detection scheme has been obtained by R. Chawla *et al.* [18] using Mamdani-type fuzzy logic image processing unit.

The speed of the micro crack detection is not the only problem associated with advanced EL imaging systems, but also the quality of the yielded image that possibly would identify and categories the cracks affecting the solar cell. A recent study by [19] and [20] discussed the potential of observing the micro cracks in 2D and 3D dimension using a multi-stage fabrication and reprocessing stages. The major drawback of these techniques that the actual output power of the affected PV cells have to be determined before the detection of the cracks is feasible, as a result this would substantially increase the computational time in order to discover the cracks location. On the other hand, an enhanced crack segmentation technique for PV micro crack detection is proposed by D. Stromer *et al.* [21]. This technique enhances the layout structure of the PV cracks, while the orientation and location yet has not been improved compared to conventional EL imaging system.

The main objective of this article is to present the development of a novel technique that is used to improve the detection of PV micro cracks using the analysis of the output image obtained by a conventional EL setup. The yielded image of the proposed technique not only enhances the interpretation of the micro cracks size, but also the improving the layout of the cracks position and orientation.

Rest of the article is organized as follows: section 2 presents the main imaging principles of conventional EL systems, while section 3 defines main problems associated with EL output images. Section 4 presents the developed method using the recombination of a binary and Fourier transform image. Last, sections 5 and 6 present the overall results and main conclusions, respectively.

## 2. Electroluminescence Imaging Principles

Electroluminescence (EL) solar cell imaging relies on the same principle as a light emitting diode (LED), where a source of current is provided into a solar cell and radiative recombination of emitted carriers causes a light emission. As an indirect bandgap semiconductor material, the peak of carrier recombination in silicon occurs through defect locations. The amount of band-to-band recombination generating radiative emission is relatively low. However, there is a small volume of radiative carrier recombination that occurs even in the silicon and this signal could be detected using an external sensor [22].

Overview of an EL system is shown in Fig. 1. The EL technique affords a means of data about the area and the location related to uniformity of solar cells. It is non-destructive and relatively fast with measurement times varying from 1 ms. ~ few seconds. The EL technique has become progressively standard practice in determining the cracks for solar cells, with the advent of low cost silicon CCD cameras available in the market [23]. EL use similar CCD cameras to the ones used for digital cameras but adjusted for better sensitivity in the near-infrared as well as cooled-down to diminish thermal noises. As with digital cameras, there are detectors with various mega-pixels resolutions of  $2048 \times 4096$  pixels enabling high resolution images of solar cell or entire PV module.

Usually, a sample holder on top of the stage is temperature controlled via peltier elements. Where a secondary water cooling is used to remove excess heat from the solar cell holder. Hence, the solar cell temperature can be regulated. In addition, a power source controlled via PC unit interface is used to bias the solar cell, optimally at short circuit current ( $I_{sc}$ ) to give the optimum recombination of the carries, hence, the detection of the EL signal is possible.

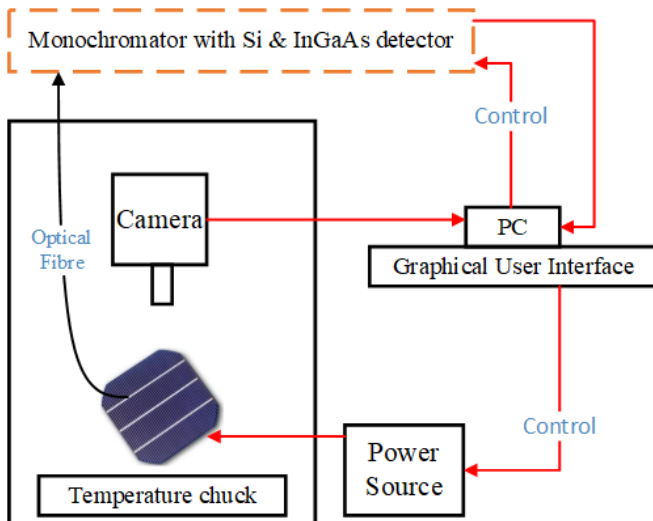


Fig. 1. Typical EL imaging system

## 3. Problem Definition

A significant drawback of a silicon detector (CCD camera) is that they have a poor response beyond 1000 nm due to the minimal absorption of the carrier recombination. An alternative detector is arrays of InGaAs photodiodes. It has a much better response over the 1000-1300 nm wavelength, this detector would qualify much faster data acquisition but with pointedly higher cost. In addition, signals of wavelengths varying from 300-900 are detected using an ultraviolet to near infrared detector [24].

The major drawback of existing micro cracks detection systems, particularly using EL aiming system, that the obtained image of the cracks does not necessary corresponds to the actual size of the crack, since EL setup would possibly add additional noise to the output detectable image. In addition, the orientation of the actual cracks are hardly to justify due to the response of the EL setup, hereby, it is worth noting that EL image is observed over a period of milliseconds, whereas for faster data acquisition it is well-know that field-programmable gate array (FPGA) tools are always recommended. Another potential drawback of conventional EL systems that they comprise low-cost detectors, hence, the micro cracks of the yielded image is barely to quantify.

An output image of typical EL setup comprising low and high resolution CCD detectors is shown in Fig. 2. As noticed, the high-resolution detector clearly justifies the location and size of the concrete cracks exists in the solar cell, whereas it is unlikely to sign the cracks using the low-resolution CCD detector. Other scanning technology such as the contact imaging sensor (CIS) detectors are available in EL systems. Instead of using a classic lens to minimize the original EL image onto the sensor, CIS technology integrates many fiber optic lenses to relocation the original image information. The biggest advantage of the CIS detectors that they are less expensive than the traditional CCD models, but they provide lower image quality, especially when it comes to detection micro cracks in solar wafer.

By contrast with above limitations, in this article we provide a novel method that is able to enhance the output image obtained using the conventional EL image using low and high cost CCD cameras. Therefore, the output image would be expected to provide a higher-quality image of the micro cracks. Furthermore, a brief overview for the key mathematical calculations is also discussed, whereas multiple examples of solar cell affected by micro cracks are also deliberated.

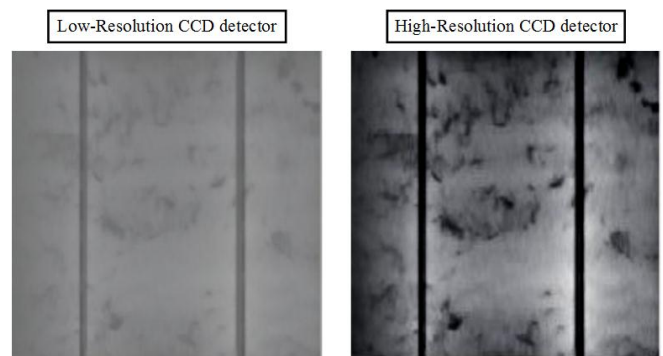


Fig. 2. Comparison of typical output image for EL setup including low and high resolution CCD detector

Our method is reliant on the detection of an EL image for cracked solar cell samples, while we did not use the Photoluminescence (PL) imaging technique as it is ideally used to inspect solar cells purity and crystalline quality for quantification of the amount of disorder to the purities in the materials. In addition, PL imaging setup is more expensive compared with traditional EL systems.

#### 4. Proposed Technique

In order to enhance the detection and the layout of the EL image, we proposed a simple and reliable method that comprises different image processing techniques. The overall structure/flowchart of the proposed technique is shown in Fig. 3. Initially, the solar cell sample will be examined under EL imaging setup, while the output image will be processed into two different methods, namely, a binary image and the Discrete Fourier Transform (DFT). In principle, the binary image is used to enhance the detection of the solar cell crack size, position and orientation, while, on the other hand, the DFT is used to map the frequency ranges of the EL image.

Next, we have used a bit-by-bit OR method that combines the output binary and DFT images to one yielded image. In order to enhance the colour mapping for the cracks, a colour coding structure has been used, nevertheless, colour coding is not a requirement to improve the quality of the EL output image, but it could be used to represent the cracks and layout of the modified image using a different colour.

In this article, the EL setup used to inspect the cracks in the examined solar cell samples comprised a digital camera “Nikon-D40-type” equipped with a standard 19-55 mm optical lens. The infrared filter was removed, hence the detection of near infrared spectrum is observed. This camera has a maximum image resolution of 6000 x 4000 with a continuous shooting speed of 5fps. The cost of this EL setup is in the range of £500~£700, depending on the source of supplier.

##### 4.1. Geometric properties of the obtained binary image

Suppose that the solar cell EL image has been determined, the next step is to recognize and locate objects within the image, ideally, the cracks in the wafer. In general, for a binary image it is well-known that the area  $A$  of the image is determined using (1).

$$A = \sum_{i=1}^{n-1} \sum_{j=0}^{m-1} B[i, j] \quad (1)$$

where  $B[i, j]$  is the two dimensional (2D) binary image. Therefore, the position of the object in the inspected EL image could be calculated using (2) and (3).

$$\bar{x} \sum_{i=1}^{n-1} \sum_{j=0}^{m-1} B[i, j] = \sum_{i=1}^{n-1} \sum_{j=0}^{m-1} j B[i, j] \quad (2)$$

$$\bar{y} \sum_{i=1}^{n-1} \sum_{j=0}^{m-1} B[i, j] = - \sum_{i=1}^{n-1} \sum_{j=0}^{m-1} i B[i, j] \quad (3)$$

where  $\bar{x}$  and  $\bar{y}$  are the coordinates of the center of the region of the cracks found in the binary image. Thus, the exact position of the cracks are determined using (4) and (5) using the analysis of the  $\bar{x}$  and  $\bar{y}$  coordinates.

$$\bar{x} = \frac{\sum_{i=0}^{n-1} \sum_{j=0}^{m-1} j B[i, j]}{A} \quad (4)$$

$$\bar{y} = \frac{- \sum_{i=0}^{n-1} \sum_{j=0}^{m-1} i B[i, j]}{A} \quad (5)$$

The challenge now is related to find the actual orientation of the observed cracks in the binary image, the position and size/area has been established, yet the orientation has to be originate. The calculations for the cracks orientation is fairly more complex compared to the position and the size. Here, we are looking at the exact orientation of a 2D-view for a crack, size the 3D-crack objects are not available using the original EL image. Thus, given the binary image  $B[i, j]$ , it is

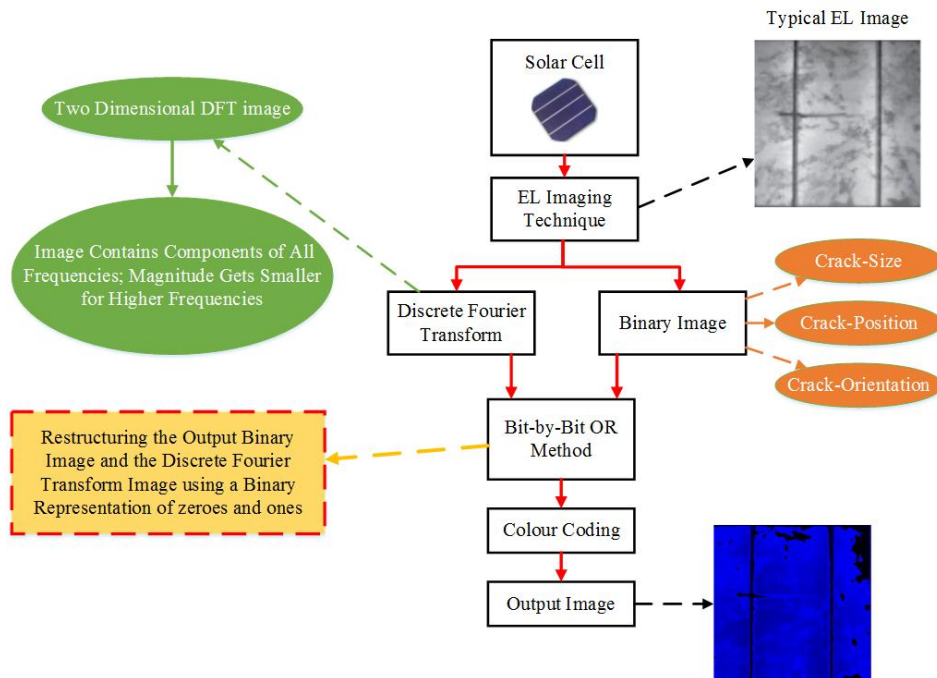


Fig. 3. Flowchart of the proposed technique



possible to compute the least squares fit for a line to the object/cracks points. This is defined as (6).

$$x^2 = \sum_{i=1}^{n-1} \sum_{j=0}^{m-1} r_{i,j}^2 B[i,j] \quad (6)$$

where  $r_{i,j}^2$  is the perpendicular distance from an object  $[i,j]$  to the actual line. It is commonly known that avoiding the numerical problem associated with the least-square fit is done using the line geometry in polar coordinates as defined by (7).

$$\gamma = x \cos \theta + y \sin \theta \quad (7)$$

where  $\theta$  is the orientation of the normal to the line with respect to x-axis, and  $\gamma$  is the distance of the line from the origin.

The distance  $r$  is of any point positioned at  $(x,y)$  coordinates is obtained by inputting the coordinates of the point into equation (7), resulting a line equation by (8).

$$r^2 = (x \cos \theta + y \sin \theta - \gamma)^2 \quad (8)$$

Therefore, it is possible plug the value of  $r^2$  into the actual least squares fit previously determined by (6). Resulting a model parameter of the angle and distance that is defined by (9).

$$x^2 = \sum_{i=1}^{n-1} \sum_{j=0}^{m-1} (x \cos \theta + y \sin \theta - \gamma)^2 B[i,j] \quad (9)$$

As can be noticed, the value of  $\theta$  is determined by the line function, the binary image is found earlier by  $B[i,j]$ , the only missing part of the formulation for the exact orientation of the cracks is the distance of the line (crack) from the origin (binary image origin),  $\gamma$ . However, this is possible to attain, simply found using (10). Where  $\bar{x}$  and  $\bar{y}$  have been already determined using (4) and (5), respectively.

$$\gamma = \bar{x} \cos \theta + \bar{y} \sin \theta \quad (10)$$

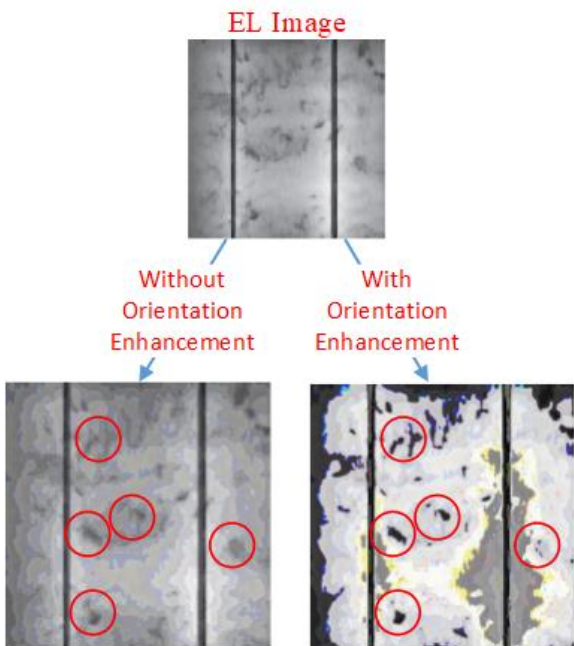


**Fig. 4.** Micro cracks orientation detection

As presented in Fig. 4, a typical EL image of a micro cracked solar cell sample is tested. Without determining the orientation of the cracks, it is clearly shown that the obtained EL image does not improve it terms of its quality as well as the detection of possible cracks in the solar cell. Equations (9) and (10) have been applied to observe the actual oriental of the cracks; hence, the overall structure of the EL image is significantly improved.

#### 4.2. Discrete Fourier Transform (DFT) image processing

The discrete Fourier Transform (DFT) is an important image-processing tool, which is used to decompose an image into its frequency response using the initial image in the form of spatial domain [25], such as a typical EL image. In this article, we have included the DFT analysis of the EL image in order to analyse the actual magnitude of the cracks, in other words, the DFT image would help to isolate the actual detected cracks from non-cracked areas, hence, it would support the identification of the cracks magnitude, size, and orientation.

The DFT has been used to analyse the EL image in two-dimensional spectrum. The output image of the DFT consists of structures of all required frequencies, while high frequencies matches a very low magnitude and low frequencies corresponds to high magnitude acquired for the EL image. For square image, such as a typical EL image, of size  $M \times N$ , the two-dimensional DFT is given by (11).

$$F(u, v) = \sum_{i=0}^{n-1} \sum_{j=0}^{n-1} f(i, j) e^{-2\pi i (\frac{ui}{M} + \frac{vj}{N})} \quad (11)$$

where  $f(i, j)$  is the actual image obtained suing the EL technique, M and N corresponds to the actual size/matrix of the EL image. Appendix A shows the actual code to implement the function using mathematical-based approach; primarily using MATLAB/Simulink software.

A typical representation of the output image for DFT is shown in Fig. 5. In most DFT implementations the output image is shifted in such a way, that the image mean at  $F(0,0)$  is displayed in the center of the image, as clearly shown in Fig. 5. The frequency response obtained using the output DFT is shown in Fig. 6. Since the original EL image shows three areas of cracks, as labeled in Fig. 6, it is expected to see that the DFT output frequency response has low frequency at these specific areas; since low frequency corresponds to higher magnitude in the actual EL image. This is confirmed using the analysis of the DFT.

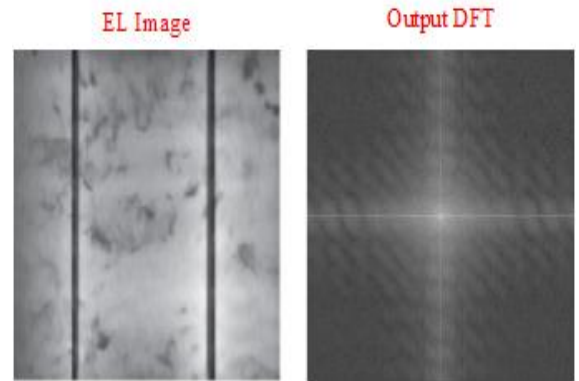


**Fig. 5.** Output image obtained using DFT

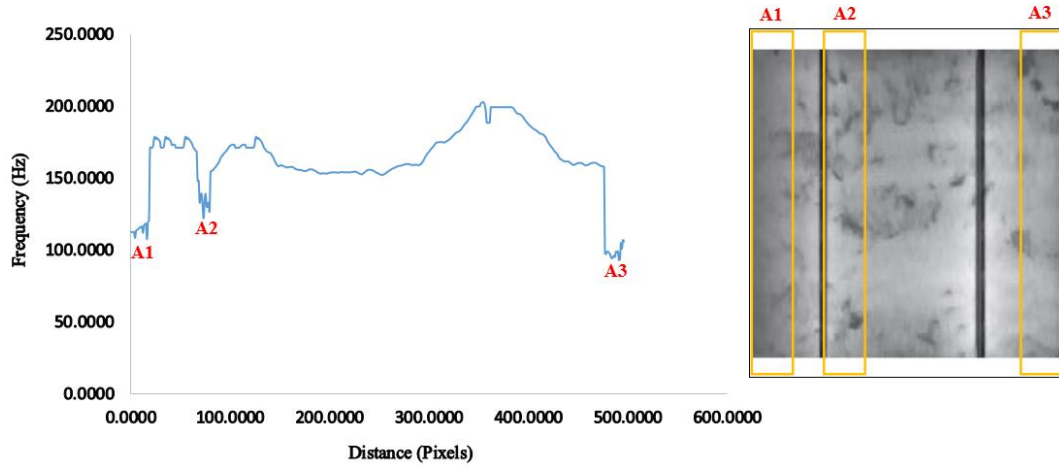


**Fig. 6.** Output frequency response determined using the DFT of the EL image; three areas of cracks have been determined and labelled on both the frequency response and the actual EL image

#### 4.3. Bit-By-Bit OR Method

After obtaining the output binary and DFT images, we have used a method, commonly known as bit-by-bit ORing, which decides the output calibrated image structure from two distinct images. The output binary and DFT images will be represented as a binary number; 0's and 1's. Where "0" corresponds to non-cracked area and "1" corresponds to an actual crack affecting the area of a particular location in the solar cell. It is worth noting that the binary levels of the DFT image is set to equal to "0" if the measured frequency is greater than 125 Hz, while at lower frequencies a binary "1" micro cracks are expected.

The bit-by-bit restructuring for the output binary and DFT images are shown in Fig. 7. The determination of the binary level of each bit could be described as follows:

- **Binary image:** the construction of each bit is observed based on the detection of possible cracks including the crack size, position and orientation. Hence, if a crack is predicted using the mathematical modeling previously discussed using (1) to (10), therefore, a binary of "1" would be generated. Otherwise, a binary "0" would be assigned to the bit.
- **DFT image:** the construction of each bit is observed using the analysis of the frequency response for the image. We have applied the condition, when the frequency is lower than 125 Hz, resulting a binary of "1", otherwise a binary of "0" would be assigned to the observed bit. It is worth noting that the threshold of 125 Hz is commonly known by the threshold of DFT, particularly applied with electroluminescence and photoluminescence images.

After determining the binary level of each bit, and OR method will be applied. It is simply built using OR gate functionality. The following condition is applied for the reconstruction of the final image:

*If output is equal to "0"*  
*{Non-cracked area is detected, represented by white colour}*  
*Else (if output is equal to "1")*  
*Cracked area is detected, represented by black colour*

A summary of the overall algorithm and the output images determined in each stage is shown in Fig. 8. Worth noting that the overall output image has better visualization of the micro cracks determined using the conventional EL image technique.

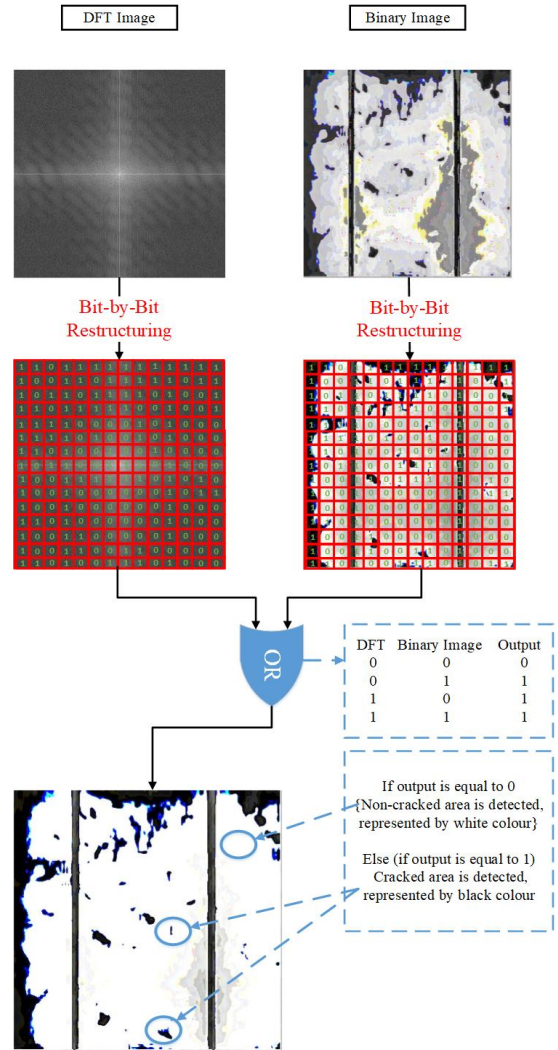


**Fig. 7.** Output image obtained using OR method between the binary and DFT image

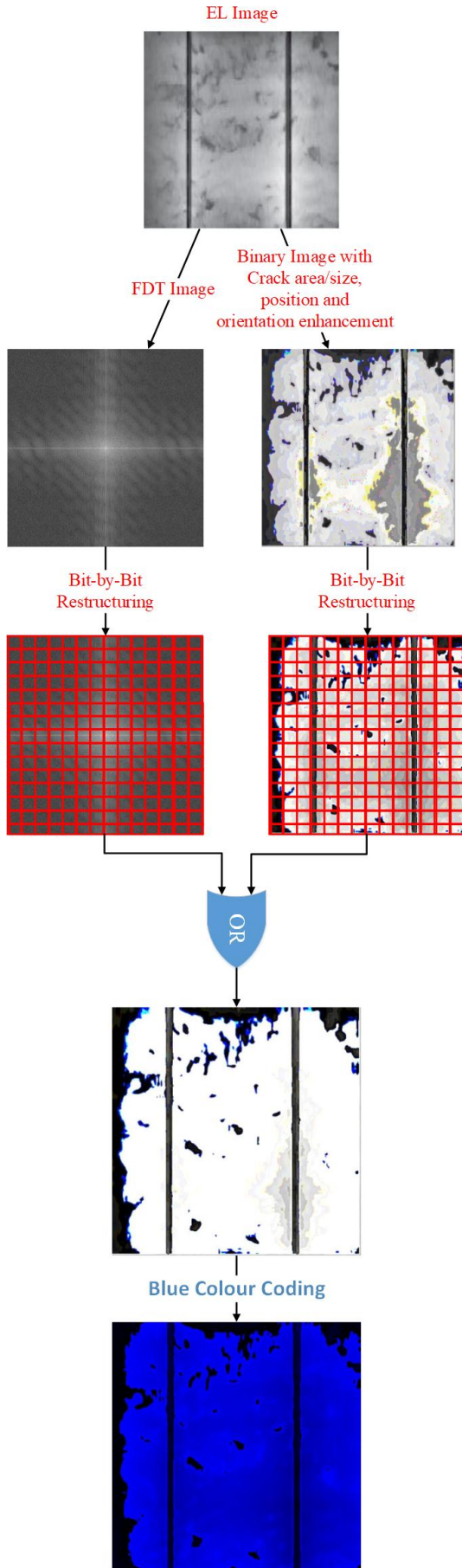


**Fig. 8.** Obtained images from each stage of the proposed micro crack detection algorithm

## 5. Results and Discussion

In this section the evaluation of the effectiveness of the proposed algorithm will be assessed using the detection of micro cracks in multiple solar cell samples. We will be comparing the difference between the obtained image using the developed algorithm vs. the conventional EL image.

According to Fig. 9, a solar cell sample has been observed using EL imaging technique. As noticed, multiple cracks appear in the EL image, where in fact, the detection of the cracks have been improved using the proposed algorithm. As labelled by the square blocks, there are multiple cracks or shade in the EL image, while after enhancing the image, it was noticed that these areas do not contain any source of cracks. On the other hand, areas labeled by the circles contain micro cracks in both the EL and output image determined using the proposed algorithm. Main problem associated with the EL image, that the actual size, position and orientation of the cracks are not clearly detected. Therefore, the output image of the proposed algorithm shows that there is a significant improvement in determining the actual size and position of each observed crack.

As a result, the output images shown in Fig. 9 proves that the actual cracks detection is more visible using the proposed method, compared to the conventional EL technique.

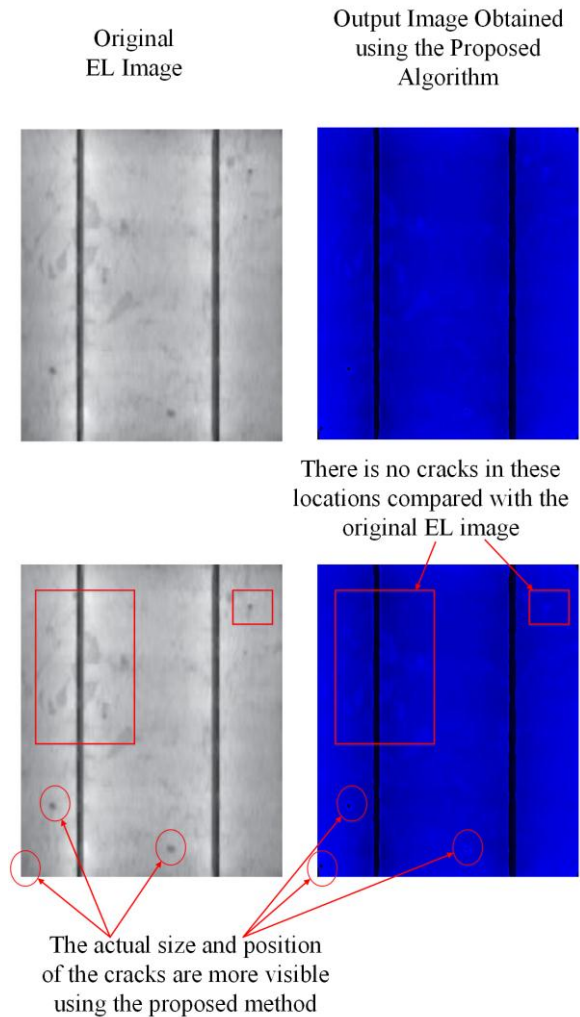


**Fig. 9.** Output image obtained using the proposed method vs. conventional EL method



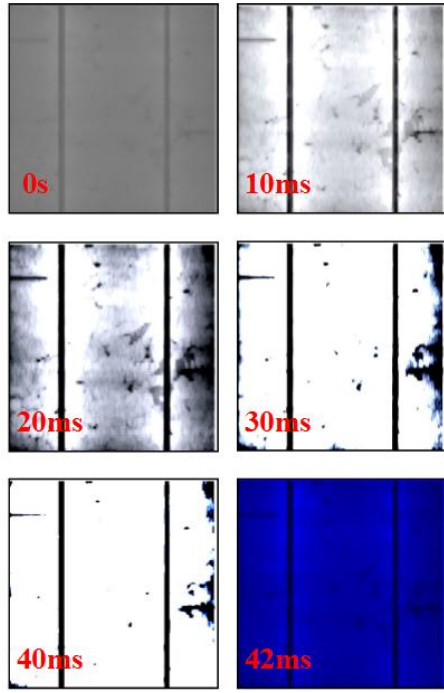


**Fig. 10.** Output images taken at different time lapse during processing of low-resolution EL image; typical speed of the detection systems is ranging from 40ms to 42ms

In order to evaluate the inspection speed of the proposed method, the output image of a cracked solar cell sample has been observed during different time succession. Fig. 10 shows a time lapse of images taken at different processing time while it took 25ms (0.025 seconds) to acquire the final calibrated image using the proposed technique, while up-to-date studies [26-29] acquire longer than 3.6s to reprocess the calibration of an EL image using different EL augmentation techniques. The typical image size is 720 x 720 pixels, typically a high-resolution image. As noticed, the crack size, position and orientation has a better feasibility while the processing time is counting. This is due to the implied calculations discussed earlier in the previous section. It is also worth mentioning that the colour mapping of the

output image often takes around 27ms, of course this time could be excluded if no colour mapping is to be established.

In contrast, the proposed technique requires 60 images of size 720 x 720 pixels to complete the inspection of the whole PV module surface that contain 60 solar cells. Only 1.62s is needed to inspect the entire solar module surface including the colour coding, and 1.5s excluding the colour coding. Hence it is fast enough for on-line and real-time solar module inspection.

A reaming question that has not been yet discussed, how long it takes to expedition the proposed method if the EL setup acquire low resolution images, typically for old EL systems? In order to answer this concern, we have used a low resolution image captured using an EL setup with low-resolution CCD detector, typical image size is 200 x 200 pixels, while a complete cycle to attain the output calibrated image during different time lapse is shown in Fig. 11.

The low-resolution image of the EL system has been processed while it took 40ms (0.04 seconds) to acquire the final image. Additional 2ms is needed to generate the colour coding image. By contrast with this result, there is additional 20ms that is needed to adjust the cracks size, position and orientation using a low-resolution EL image.

## 6. Comparative Study

In order to verify the effectiveness of the proposed micro crack detection technique, the obtained results have been compared with multiple [7] and [26]-[29] well-developed micro cracks detection methods. A summary of the comparison is shown in Table I.

According to [26] and [28], both developed methods custom the detection of micro cracks using a Photoluminescence (PL) imaging technique. In fact, the PL signal is determined by the actual lifetime which is mostly affected by both bulk and surface recombination, and when during high spatial resolution and short measurement time, the PL imaging can be used inline during the production of silicon wafers. For example, in [26], the developed detection method enhanced the PL imaging technique using a contact less modulation for the actual obtained PL images, while a complex optical sensor and LED-based driver have to be used.

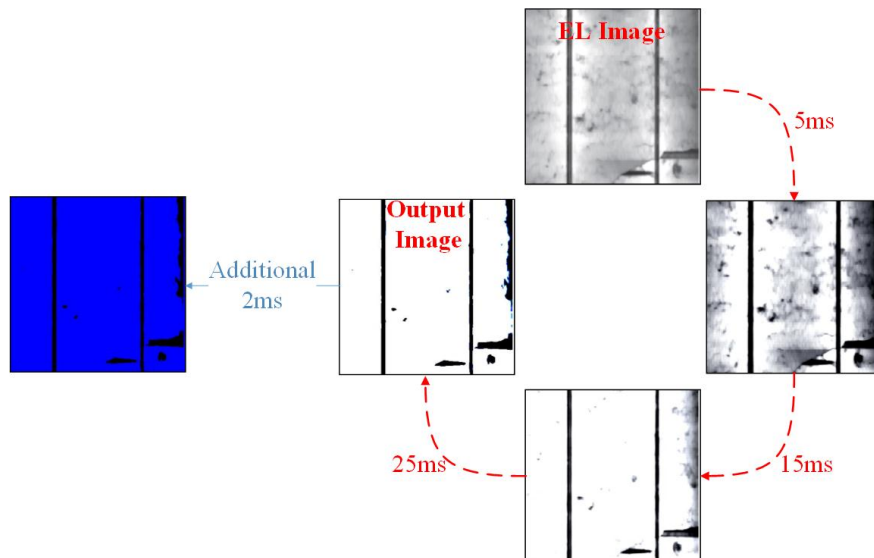


**Fig. 11.** Output images taken at different time lapse during processing of high-resolution EL image; typical speed of the detection systems is ranging from 25ms to 27ms



On the other hand, in [28], the output PL image has been improved using analysis of the fill-factor and solar cell open circuit voltage. This would limit the detection area up to 90%, and it is quite complex in terms of the technique application, especially using micro cracks inline detection that is incorporated within the solar cells' manufacturing system, since main electrical parameters such as open circuit voltage and fill factor are required.

Other micro cracks detection techniques use thermal imaging such as the well-developed method proposed by W. Brooks et al. [27]. This method can identify the noninvasive and nondestructive regions of the inspected solar cell samples. Main limitations associated with this method that is has to use a high-resolution IR camera, and there is no evidence that this technique would identify micro cracks in the range of 100µm.

Recently, multiple methods are capable of detecting micro cracks of solar cell wafers using the concept of EL imaging. In [17], an automatic defect detection scheme based on Haar-like feature extraction is developed. This method also uses a fuzzy C-means algorithms in order to enhance the layout of the detected EL image. The method is quite stable and it has a fast response in determining the output EL image. However, two automatic parameters including the distance and fuzzy clusters are needed prior to the inspection of the cracks as well as a number of crack-free and cracked solar cell samples that are required for tanning purposes. Furthermore, M. Frazão et al. [29] developed a new approach that is capable to enhance the detection of solar cells micro cracks using EL imaging technique. Main limitations associated with this method that it requires the input of two images determined using two temperature levels of 90 °C and

22 °C; this condition is not available during the manufacturing executing systems for solar cell wafers.

By contrast with above limitations, in this article, we proposed a reliable and simple mathematical-based method to enhance the detection of micro cracks using the reprocessed image of a conventional EL setup. Here, we developed the algorithm using binary and DTF image processing models that enables the enhancement of the micro cracks size, position and orientation. While the only limitation associated with the developed technique that it requires to incorporate various mathematical calculations in order to successfully function the micro cracks detection.

## 7. Conclusion

In this article, we presented the advancement of a cutting edge technique that is used to enhance the detection of micro cracks in solar cells. The output image of a conventional electroluminescence (EL) system is determined and reprocessed using a binary and DFT image refinement models. The suggested procedure can effectively enhance the detection of the micro cracks size, position and orientation.

The detection method mainly focuses on deploying mathematical-based model to the existing EL systems setup; while to process the enhancing the detection of micro cracks for a full-scale PV module containing 60 solar cells it would typically take around 1.62s and 2.52s for high and low resolution EL images, respectively. We have used a colure-coding structure for the output obtained images. This procedure is not a requirement to function the proposed technique, but it helps to outline cracks, and possibly could be used in the future in different imaging enhancement applications.

Table I Comparative results between the proposed method and the one presented in [17] and [26]-[29]

| Ref.            | Year of the study | Technique |    |                 | Technique Description   | Major Limitation  | Typical Detection Speed for 60 solar cells                          |
|-----------------|-------------------|-----------|----|-----------------|---|---|---|
|                 |                   | EL        | PL | Thermal-Imaging |   |   |   |
| [27]            | 2015              | x         | x  | ✓               | Noninvasive and nondestructive method of crack detection in crystalline Si solar cells using thermal imaging camera.  | Expensive equipment is required such as high-resolution IR camera.  | N/A   |
| [17]            | 2015              | ✓         | x  | x               | An automatic defect detection scheme based on Haar-like feature extraction and a new clustering technique is developed. A Fuzzy C-means is used to enhance the image processing time. | Multiple crack-free and cracked solar cell samples are required to for the training purposes.                         | 3.6 seconds   |
| [28]            | 2016              | x         | ✓  | x               | The technique uses the analysis of the fill-factor and solar cell open circuit voltage for improving the detection quality of PL and EL images.                                       | The technique need further inspection of the solar cell main electrical parameters.                                   | In the range of 1-2 minutes   |
| [26]            | 2017              | x         | ✓  | x               | An outdoor PL imaging system is proposed using a contact less modulation technique.   | Optical sensors and LED driver are required to function the PL system.  | N/A   |
| [29]            | 2017              | ✓         | x  | x               | The proposed technique uses the analysis of the EL images at high and low temperature variations.   | This technique requires the images of the inspected solar cell at two different temperature levels (90 °C and 22 °C). | In the range of 2-3 minutes   |
| Proposed Method | 2019              | ✓         | x  | x               | Binary and discreet Fourier transform (DFT) image processing models are used to enhance the image obtained by the conventional EL setup.  | Mathematical calculations have to be incorporated within the EL setup   | 1.62s and 2.52s for high and low resolution EL images, respectively |

## 8. References

- [1]. M. Dhimish, P. Mather, V. Holmes, M. Sibley, CDF modelling for the optimum tilt and azimuth angle for PV installations: case study based on 26 different locations in region of the Yorkshire UK, IET Renewable Power Generation. 13 (2018) 399-408. <http://dx.doi.org/10.1049/iet-rpg.2018.5301>.
- [2]. S.Kaplanis, E. Kaplani, Energy performance and degradation over 20 years performance of BP c-Si PV modules, Simulation Modelling Practice and Theory. 19 (2011) 1201-1211. <https://doi.org/10.1016/j.simpat.2010.07.009>.
- [3]. F. Grimaccia, S. Leva, A. Niccolai, PV plant digital mapping for modules' defects detection by unmanned aerial vehicles, IET Renewable Power Generation, 11 (2017), 1221-1228. <http://dx.doi.org/10.1049/iet-rpg.2016.1041>.
- [4]. J. Fan, D. Ju, X. Yao, Z. Pan, M. Terry, W. Gambogi, K. Stika, J. Liu, W. Tao, Z. Liu, Y. Liu, Study on snail trail formation in PV module through modeling and accelerated aging tests, Solar Energy Materials and Solar Cells. 164 (2017) pp.80-86. <https://doi.org/10.1016/j.solmat.2017.02.013>.
- [5]. M. Koehl, M. Heck, S. Wiesmeier, Modelling of conditions for accelerated lifetime testing of Humidity impact on PV-modules based on monitoring of climatic data, Solar Energy Materials and Solar Cells. 99 (2012) 282-291. <https://doi.org/10.1016/j.solmat.2011.12.011>.
- [6]. M. Dhimish, Micro cracks distribution and power degradation of polycrystalline solar cells wafer: Observations constructed from the analysis of 4000 samples, Renewable Energy. 145 (2020) 466-477. <https://doi.org/10.1016/j.renene.2019.06.057>.
- [7]. M. Dhimish, V. Holmes, P. Mather, Novel Photovoltaic Micro Crack Detection Technique, IEEE Transactions on Device and Materials Reliability. 19 (2019) 304-312. <https://doi.org/10.1109/TDMR.2019.2907019>.
- [8]. M. Dhimish, P. Mather, Development of Novel Solar Cell Micro Crack Detection Technique, IEEE Transactions on Semiconductor Manufacturing. 32 (2019) 277-285. <https://doi.org/10.1109/TSM.2019.2921951>.
- [9]. M. Köntges, I. Kunze, S. Kajari-Schröder, X. Breitenmoser, B. Bjørneklett, The risk of power loss in crystalline silicon based photovoltaic modules due to micro-cracks, Solar Energy Materials and Solar Cells, 95 (2011) 1131-1137. <https://doi.org/10.1016/j.solmat.2010.10.034>.
- [10]. M. Dhimish, V. Holmes, M. Dales, B. Mehrdadi, Effect of micro cracks on photovoltaic output power: case study based on real time long term data measurements, Micro & Nano Letters, 12 (2017) 803-807. <http://dx.doi.org/10.1049/mnl.2017.0205>.
- [11]. A. Dolar, S. Leva, G. Manzolini, E. Ogliari, Investigation on performance decay on photovoltaic modules: Snail trails and cell microcracks, IEEE journal of photovoltaics. 4 (2014) 1204-1211. <https://doi.org/10.1109/JPHOTOV.2014.2330495>.
- [12]. M. Florides, G. Makrides, G.E. Georgiou, Early Detection of Potential Induced Degradation by Measurement of the Forward DC Resistance in Crystalline PV Cells, IEEE Journal of Photovoltaics. 9 (2019) 942-950. <https://doi.org/10.1109/JPHOTOV.2019.2910235>.
- [13]. M. Dhimish, V. Holmes, B. Mehrdadi, M. Dales, The impact of cracks on photovoltaic power performance, Journal of Science: Advanced Materials and Devices. 2 (2017) 199-209. <https://doi.org/10.1016/j.jsamd.2017.05.005>.
- [14]. M. Bliss, X. Wu, K.G. Bedrich, J.W. Bowers, T.R. Betts, R. Gottschalg, Spatially and spectrally resolved electroluminescence measurement system for photovoltaic characterization, IET Renewable Power Generation. 9 (2015) 446-452. <https://doi.org/10.1049/iet-rpg.2014.0366>.
- [15]. M. Dhimish, V. Holmes, B. Mehrdadi, M. Dales, P. Mather, PV output power enhancement using two mitigation techniques for hot spots and partially shaded solar cells, Electric Power Systems Research. 158 (2018) 15-25. <https://doi.org/10.1016/j.epsr.2018.01.002>.
- [16]. W. Muehleisen, G.C. Eder, Y. Voronko, M. Spielberger, H. Sonnleitner, K. Knoeb, R. Ebner, G. Ujvari, C. Hirschl, Outdoor detection and visualization of hailstorm damages of photovoltaic plants, Renewable energy. 118 (2018) 138-145. <https://doi.org/10.1016/j.renene.2017.11.010>.
- [17]. D.M. Tsai, G.N. Li, W.C. Li, W.Y. Chiu, Defect detection in multi-crystal solar cells using clustering with uniformity measures, Advanced Engineering Informatics. 29 (2015) 419-430. <https://doi.org/10.1016/j.aei.2015.01.014>.
- [18]. R. Chawla, P. Singal, A.K. Garg, A Mamdani Fuzzy Logic System to Enhance Solar Cell Micro-Cracks Image Processing, 3D Research. 9 (2018), p.34. <https://doi.org/10.1007/s13319-018-0186-7>.
- [19]. M. Dhimish, V. Holmes, P. Mather, C. Aissa, M. Sibley, Development of 3D graph-based model to examine photovoltaic micro cracks, Journal of Science: Advanced Materials and Devices. 3 (2018) 380-388. <https://doi.org/10.1016/j.jsamd.2018.07.004>.
- [20]. M. Dhimish, G. Badran, Current limiter circuit to avoid photovoltaic mismatch conditions including hot-spots and shading, Renewable Energy. 145 (2020) 2201-2216. <https://doi.org/10.1016/j.renene.2019.07.156>.
- [21]. D. Stromer, A. Vetter, H.C. Oezkan, C. Probst, A. Maier, Enhanced Crack Segmentation (eCS): A Reference Algorithm for Segmenting Cracks in Multicrystalline Silicon Solar Cells, IEEE Journal of Photovoltaics. 9 (2019) 752-758. <https://doi.org/10.1109/JPHOTOV.2019.2895808>.
- [22]. B. Doll, T. Pickel, O. Schreier, C. Zetzmann, J. Hepp, J. Teubner, C. Buerhop, J.A. Hauch, C. Camus, C.J. Brabec, High-throughput, outdoor characterization of photovoltaic modules by moving electroluminescence measurements, Optical Engineering. 58 (2019) 083105. <https://doi.org/10.1117/1.OE.58.8.083105>.
- [23]. W. Muehleisen, C. Hirschl, G. Brantegger, L. Neumaier, M. Spielberger, H. Sonnleitner, B. Kubicek, G. Ujvari, R. Ebner, M. Schwark, G.C. Eder, Scientific and economic comparison of outdoor characterisation methods for photovoltaic power plants, Renewable energy. 134 (2019) 321-329. <https://doi.org/10.1016/j.renene.2018.11.044>.
- [24]. H.L. Zhu, Z. Liang, Z. Huo, W.K. Ng, J. Mao, K.S. Wong, W.J. Yin, W.C. Choy, Low-Bandgap Methylammonium-Rubidium Cation Sn-Rich Perovskites for Efficient Ultraviolet-Visible-Near Infrared Photodetectors, Advanced Functional Materials. 28 (2018) 1706068. <https://doi.org/10.1002/adfm.201706068>.
- [25]. T. Bekkouche, S. Bouguezel, Digital double random amplitude image encryption method based on the symmetry property of the parametric discrete Fourier transform, Journal of Electronic Imaging. 27 (2018) 023033. <https://doi.org/10.1117/1.JEI.27.2.023033>.
- [26]. R. Bhoopathy, O. Kunz, M. Juhl, T. Trupke, Z. Hameiri, Outdoor photoluminescence imaging of photovoltaic modules with sunlight excitation, Progress in Photovoltaics: Research and Applications. 26 (2018) 69-73. <https://doi.org/10.1002/pip.2946>.
- [27]. W.S. Brooks, D.A. Lamb, S.J. Irvine, IR reflectance imaging for crystalline Si solar cell crack detection, IEEE Journal of Photovoltaics. 5 (2015) 1271-1275. <https://doi.org/10.1109/JPHOTOV.2015.2438636>.
- [28]. O. Nos, W. Favre, F. Jay, F. Ozanne, A. Valla, J. Alvarez, D. Muñoz, P.J. Ribeyron, Quality control method based on photoluminescence imaging for the performance prediction of c-Si/a-Si: H heterojunction solar cells in industrial production lines, Solar Energy Materials and Solar Cells. 144 (2016) 210-220. <https://doi.org/10.1016/j.solmat.2015.09.009>.
- [29]. M. Frazão, J.A. Silva, K. Lobato, J.M. Serra, Electroluminescence of silicon solar cells using a consumer grade digital camera, Measurement. 99 (2017) 7-12. <https://doi.org/10.1016/j.measurement.2016.12.017>.